Lab on a Chip

RSC Publishing

PAPER

Single particle detection, manipulation and analysis with resonant optical trapping in photonic crystals†

Cite this: *Lab Chip*, 2013, **13**, 3268

Nicolas Descharmes, Ulagalandha Perumal Dharanipathy, Zhaolu Diao, Mario Tonin and Romuald Houdré

Received 10th April 2013,
Accepted 21st May 2013

DOI: 10.1039/c3lc50447f

www.rsc.org/loc

We demonstrate a resonant optical trapping mechanism based on two-dimensional hollow photonic crystal cavities. This approach benefits simultaneously from the resonant nature and unprecedented field overlap with the trapped specimen. The photonic crystal structures are implemented in a 30 mm × 12 mm optofluidic chip consisting of a patterned silicon substrate and an ultrathin microfluidic membrane for particle injection and control. Firstly, we demonstrate permanent trapping of single 250 and 500 nm-sized particles with sub-mW powers. Secondly, the particle induces a large resonance shift of the cavity mode amounting up to several linewidths. This shift is exploited to detect the presence of a particle within the trap and to retrieve information on the trapped particle. The individual addressability of multiple cavities on a single photonic crystal device is also demonstrated.

Introduction

Optical tweezers as demonstrated by Ashkin and Dziedzic[1,2] has been widely applied in a variety of physical[3–5] and biological studies.[6,7] It would be of high interest to extend the features of these free space tweezers onto an integrated platform for two major reasons. Firstly, the ability of miniaturization to replicate the current functionalities on a single chip minimises the need for bulk optics. Secondly, to overcome the Abbe's diffraction limit that prevents the trapping of smaller sized particles such as proteins and viruses with reasonable powers. The demonstration of such an integrated counterpart of free space optical tweezers is a goal that has been a long pursued by various research groups.[8–12] There have been many applications predominantly exploiting the evanescent field of an optical mode in waveguides and in cavities.[13–15] The major limitation of these approaches lies in the fact that the overlap of the optical field on the particle is minimal, requiring the use of very large input powers. An ideal integrated optical trap would make use of ultralow trapping powers, be able to keep the particle suspended away from any surface, be exclusive[16] and be particle specific.

In this work, we make use of an integrated optical trap based on a hollow photonic crystal (HPhC) optical nanocavity[17–19] that can trap a particle within a stable volume at sub-mW trapping powers. This is achieved by simultaneously exploiting the resonant and hollow natures of the cavity.[20] The nature of this cavity permits the storing of optical energy beyond diffraction limits and the hollow volume allows for a maximum overlap of the particle with the confined optical field. This arrangement leads to the interplay between the trapped particle and the trapping field forming the basis of Self Induced Trapping (SIT).[21] The dependence of SIT on the particle-induced perturbation renders it intrinsically exclusive and particle specific, features that are beyond the reach of standard optical tweezers.[16] This perturbation, when measured could also provide interesting and relevant information on the particle under study.

Here, we present the permanent optical trapping of dielectric particles of 250 nm and 500 nm diameters with trapping powers as low as 360 μW and 120 μW respectively. We also propose and experimentally demonstrate a single particle detector that can enumerate and track particles. Finally we extend the trapping scheme to incorporate the addressability of multiple traps with different wavelengths. We also give proposals for the size, shape and refractive index specific trapping of particles using our resonant optical trap.

Methods

The HPhC cavity consists of a circular defect[17] of 700 nm in a hexagonal lattice of a 2D photonic crystal (PhC) membrane as seen in Fig. 1(b). The cavities are integrated within an optofluidic[22–28] chip of 30 × 12 mm (see Fig. 1(c)) comprising of a silicon substrate and an ultrathin PDMS membrane dedicated to the transport and control of the particles as shown in Fig. 1(d) and the ESI†. The structures are fabricated on a Silicon-On-Insulator (SOI) wafer. It consists of a 220 nm silicon layer and a 2 μm sacrificial silica layer on the silicon

Institut de Physique de la Matière Condensée, École Polytechnique Fédérale de Lausanne (EPFL), Station 3, CH-1015 Lausanne, Switzerland

† Electronic supplementary information (ESI) available. See DOI: 10.1039/c3lc50447f

This journal is © The Royal Society of Chemistry 2013

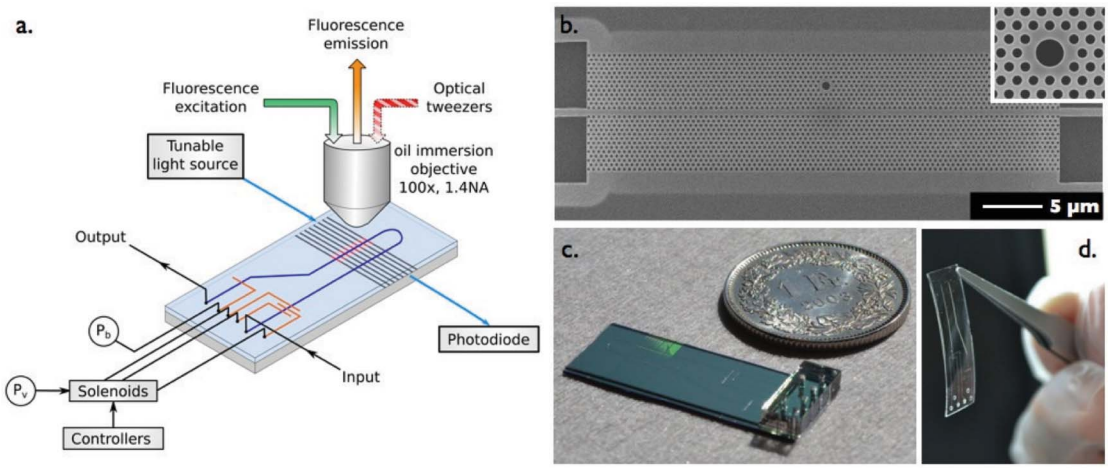

Fig. 1 (a) Schematic of the optofluidic chip and the experimental setup. (b) Scanning electron micrograph of a HPhC structure, lattice constant 420 nm, filling factor 30%, showing the circular cavity side-coupled with a PhC W1 waveguide. (c) Photograph of the optofluidic chip when fully assembled. The chip dimensions are 30 × 12 × 1.5 mm excluding the 4 mm thick PDMS interconnect. (d) Photograph of the ultrathin PDMS membrane, 170 µm thick, before positioning.

substrate. The photonic crystal pattern is first defined with a resist (ZEP520) with the aid of electron beam lithography. After development, the pattern is further transferred onto the silicon layer by dry etching with a gas mixture of SF_6 and C_4F_8. The final step consists of the removal of the sacrificial SiO_2 layer by buffered hydrofluoric acid wet etching leaving a free standing PhC membrane of 220 nm.

The PDMS membrane shown in Fig. 1(d) serves two major functions. Firstly, it allows for the accurate injection and transport of the nanoparticles towards the optical cavities and secondly, it maintains high quality optical imaging from the top of the sample. It is fabricated following standard soft lithography processes.[29] A first PDMS layer, 30 µm thick, is spin coated onto a silicon wafer comprising a positive photoresist (AZ9260) mould. Meanwhile, a second PDMS membrane, 140 µm thick, is spin coated onto a negative photoresist (SU8) mould on a silicon wafer. The thicker layer, including the control channels, is then deposited on the thinner layer, which carries the infiltration channel (120 nL). The total microfluidic layer that has been developed is considerably thinner than standard approaches and hence offers great advantages in terms of the footprint of the final device. The flexibility and deformability of the thin PDMS membrane means it must be handled very carefully. Nevertheless, it still proves to be compatible with valve actuation either in standard or peristaltic mode. The assembled microfluidic layer is finally aligned and placed on the photonic crystal chip and a 4 mm thick PDMS interconnect is added to allow stable injection and pressure control.

The schematic of the experimental setup is shown in Fig. 1(a). The assembled optofluidic chip is connected to a fibre-coupled tuneable laser diode around 1.5 µm. The laser light is injected into the optofluidic chip using tapered optical fibres. The light is then guided towards the photonic crystal structures through a ridge waveguide. A W1 waveguide,[30] which consists of a missing row of holes within the 2D triangular lattice, allows the laser excitation to be guided through the PhC structure, as seen in Fig. 1(b). A large proportion of the light confined in the waveguide couples to the hollow cavity through evanescent side coupling. More details on photonic crystal cavity-waveguide coupling can be found in the literature.[31] The light transmitted through the PhC structures is then extracted following a similar path at the other end of the device and directed towards a near-infrared detector where the signal is recorded. In the meantime, fluorescent imaging of the nanoparticles near the cavities is performed. An Argon laser (emission wavelength: 488 nm) is used to excite the fluorescence of the particles. The fluorescence emission centred on 570 nm is collected through an oil immersion objective (Leica, 100×, numerical aperture 1.4) and imaged onto an EMCCD camera (ImagEM 512, Hamamatsu). This configuration allows for a sub-20 nm resolution tracking of the centroid position of the particles at frame rates of over 100 frames per second (fps). Finally, the ultrathin microfluidic membrane allows complex manipulation of particles between different cavities with the aid of auxiliary optical tweezers (Ti:sapphire laser, emission wavelength 850 nm).

The experiment is performed as follows: a diluted solution of polystyrene particles (refractive index 1.59) is injected inside the microfluidic channel using a slight overpressure of 4 PSI. The velocity of the particles at this stage, without extra flow control can reach several millimetres per second. It is therefore crucial to be able to slow down and eventually arrest the flow of particles in the vicinity of the HPhC devices. A set of pneumatically controlled valves[29] positioned above the entrance and exit of the channel has been integrated for this purpose. Typical working pressures of 7 PSI are usually more than enough to arrest the particles, leaving them in their natural Brownian motion. Peristaltic actuation of these valves also allows for controlled injection of the particles in volumes of the order of 500 pL per cycle. In the meantime, the HPhC

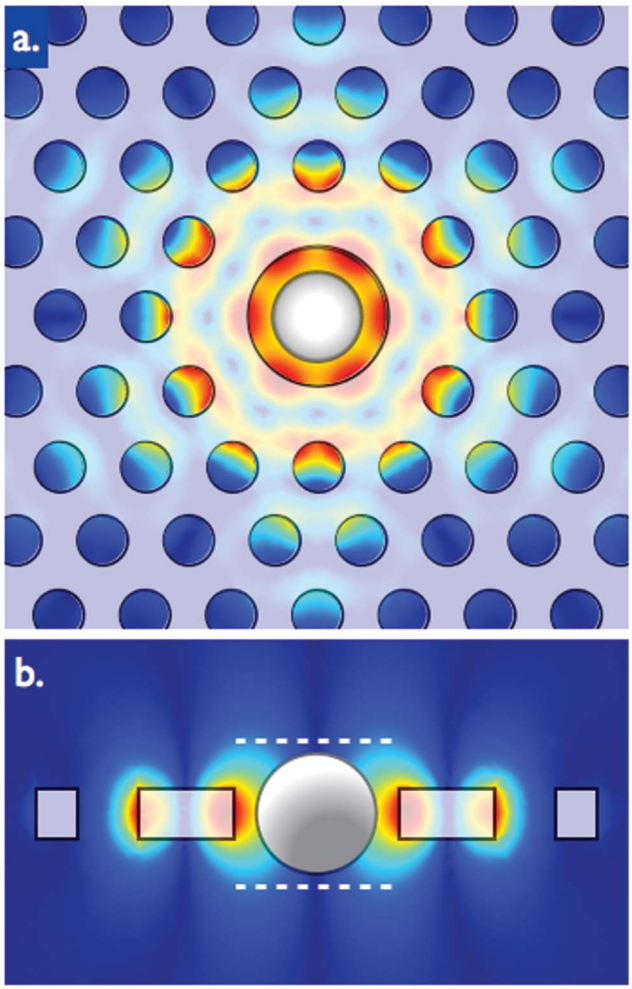

Fig. 2 FEM computation of the electric field distribution with a 500 nm particle placed in the centre of the cavity. (a) In-plane cross section showing the large overlap of the electromagnetic field with the particle. (b) Vertical cross section showing the out-of-plane extent of the cavity field. The dotted white lines represent the limits of the trapping volume.

cavities are resonantly excited through the side coupled optical fibres. At this juncture, the particles are either free to be trapped by the confined optical field (Fig. 2) in the cavity volume or can be directed towards the HPhC cavity by auxiliary optical tweezers operating from the top.

Results and discussion

Single particle trapping

When a particle is hovering in the neighbourhood of the cavity, while being resonantly excited, the optical gradient force pulls the particle towards the central region of the cavity. At appropriate excitation powers, it can then remain stably trapped for very long times in the order of tens of minutes without any sign of apparent structural damage or photobleaching. This can be observed in Fig. 3 and movies S1 and S2 (see ESI†). It is possible to accurately evaluate the amount of guided power in the W1 waveguide next to the cavity using the experimental values for waveguide propagation losses and reflection coefficients at the interfaces. Estimated guided powers as low as 120 μW for 500 nm particles were sufficient to maintain stable trapping for tens of minutes. In comparison with standard optical tweezers, this corresponds to a decrease in trapping power of approximately three orders of magnitude.[32] As can be seen in the supplementary videos,† the circular cavity allows for the trapping of only one particle at a given time. This exclusivity arises due to three factors. Firstly, the geometric limitation imposed by the circular cavity permits only a single particle in the stable region. Secondly, the trapping volume comprises of a cylinder (radius: 350 nm, height: 600 nm, volume: 0.2 μm) corresponding to the volume where the particle experiences strong optical forces. Thirdly, in the presence of two or more particles, the perturbation caused by the addition of dielectric material in the cavity would cause a large shift in the resonance wavelength resulting in the decoupling of optical energy, which eventually scales down the optical forces rapidly.

Single particle detection

The refractive index contrast due to the presence of a single dielectric particle inside the cavity volume creates an instantaneous perturbation of the eigenmode. One manifestation of this perturbation is a red-shift of the resonance wavelength of the cavity.

The magnitude of this shift is a function of the cavity field overlap with the particle and therefore it depends on the size, refractive index and shape. This shift can amount to several cavity linewidths. In our experiment,[20] for a quality factor (Q) of 2000 in water, equivalent to a cavity linewidth of 0.8 nm, the maximum resonant shift observed due to the particle presence is around 1.8 nm. This corresponds to more than twice the cavity linewidth. Consequently, for an appropriately detuned wavelength, it is possible to record large dynamic changes in the power transmitted through the device, as can be observed in Fig. 4(a). For instance, by exciting the HPhC cavity at the empty resonance wavelength, a particle traversing the hollow region will generate a sharp spike in the transmission signal as seen in Fig. 4(b). Integrating this transmission signal with a simple digital counter can provide a very efficient platform for single particle detection and enumeration. In addition, the motion of the particle within the cavity volume can also be tracked with the prior knowledge of the relationship between the position of the particle and the induced perturbation as shown in Fig. 4(c). This interesting feature brings noise spectrum analysis and feedback stabilized optical trapping within reach.

Particle-cavity back-action and 1D optical cage

The resonant nature of the trap gives rise to particularly interesting properties. Most significantly, it is possible to trap a particle in a spectral region spanning only a few cavity linewidths. The mutual interaction between the cavity field and the trapped particle, results in the fact that this spectral region is not centred on the empty resonance wavelength but on a red-shifted value of more than one linewidth for the 500 nm sized particle. In addition, the power required for stable

 This journal is © The Royal Society of Chemistry 2013

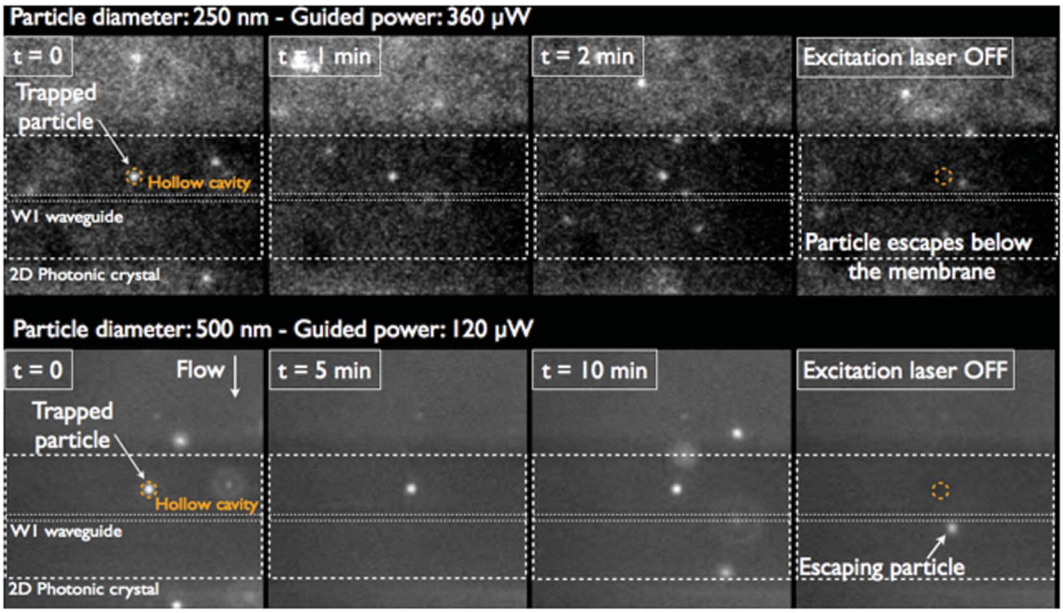

Fig. 3 Resonant optical trapping in a HPhC. (a) Optical trapping of a 250 nm particle in a hollow cavity. The particle is held within the cavity with an estimated guided power of 360 μW. The particle is steadily held for 2 min before the resonant excitation is switched off, allowing the particle to escape. (b) Optical trapping of a 500 nm particle. The same experiment as in (a) is reproduced with a larger particle for 10 min. The difference in contrast between (a) and (b) arises from the fact that the smaller particles possess fewer fluorescent markers.

trapping reaches a minimum when the excitation laser is detuned by approximately one cavity linewidth. This can be understood *via* the mechanism illustrated in Fig. 5. It has been measured experimentally that a particle located in the centre of the cavity volume shifts the resonant wavelength of the system by more than two linewidths.

As illustrated in Fig. 5(a), a one-linewidth detuned excitation couples only minimal energy to the cavity mode. As a consequence, the particle experiences a very small electromagnetic field and almost no optomechanical forces. If the particle is displaced towards the outer region, the particle induced shift decreases rapidly, leading to an increase of energy in the cavity mode and hence the build up of a restoring force, pulling the particle back to the central region (Fig. 5(b)). This intricate phenomenon can be visualized as a 1D optical cage. This novel trapping mechanism is capable of holding a particle trapped in a volume in suspension while, at the same time, exposing it to very little optical energy on average.

Single particle manipulation and analysis

In the previous section, we have demonstrated the principle behind a single hollow cavity detecting and trapping particles exclusively. Extending this feature to multiple traps is made possible by appropriately placing other cavities in the same PhC device. For instance, a 10 × 12 mm on-chip active region comprises of 100 PhC devices. Any of these devices, 100 μm long, could potentially hold up to 20 individually addressable cavities, separated in the wavelength spectrum by more than a full cavity linewidth. In Fig. 6, the trapping operation involving two such neighbouring cavities is shown. Here, two cavities are adjacently placed with their resonances separated by a few linewidths (10 nm). The particle is stably trapped in the first cavity at its corresponding resonance wavelength (1568 nm) and is released as soon as the excitation wavelength is changed to that of the resonance of the second cavity (1578 nm). Similar behaviour can be observed for the second cavity. This configuration along with the compatibility of the chip operating with auxiliary optical tweezers through the thin microfluidic membrane opens the door to complex manipulation schemes.

Discussion

The amount of perturbation caused by the particle to the cavity is central to the features demonstrated above. The differentiation of this perturbation allows the detection and trapping of the particle by merely adjusting the excitation wavelength. In Fig. 7, the variation of the cavity resonance to particle size, refractive index and shape has been numerically computed and clearly illustrates this trend. The addition of a single dielectric particle within the cavity volume creates a local perturbation that affects the eigenfrequency of the system. This results in a red-shift of the resonance wavelength of the cavity mode. The FEM solver solves for the global eigenfrequency of the cavity-particle system by solving the Maxwell's equations in the computational volume. It is possible to obtain the resonance shifts by tracking this global eigenfrequency for different values of the refractive index of the particle. It is important to note that in the case of a single 500 nm particle, the resonance shift lies in the order of the experimental cavity linewidth of 0.8 nm. This is well within the reach of the

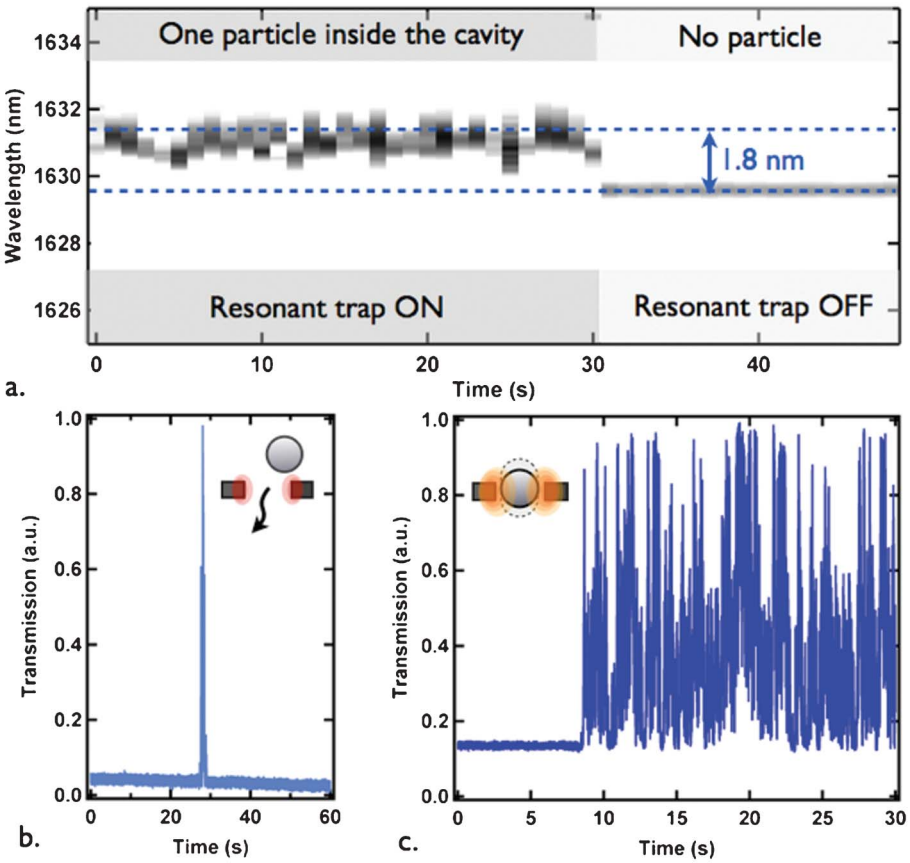

Fig. 4 Single particle detection and tracking. (a) Dynamic resonance wavelength shift recorded over time as a particle is resonantly trapped inside the cavity. The greyscale image corresponds to the record of the transmitted power through the HPhC structure. The darkest region denotes a dip in transmission associated with the instantaneous position of the resonance wavelength. An experimental red-shift of 1.8 nm is recorded. (b) Experimental record of transmission through the structure when a particle is moving swiftly through the cavity as illustrated in the inset. The input wavelength is red detuned from the empty resonance and the power is below the trapping threshold. (c) Experimental record of transmission through the structure when a particle is trapped inside the cavity. The input wavelength is red detuned from the empty resonance but the power is above the trapping threshold. The observed fluctuations are the signature of the constrained Brownian motion of the particle in the resonant trap.

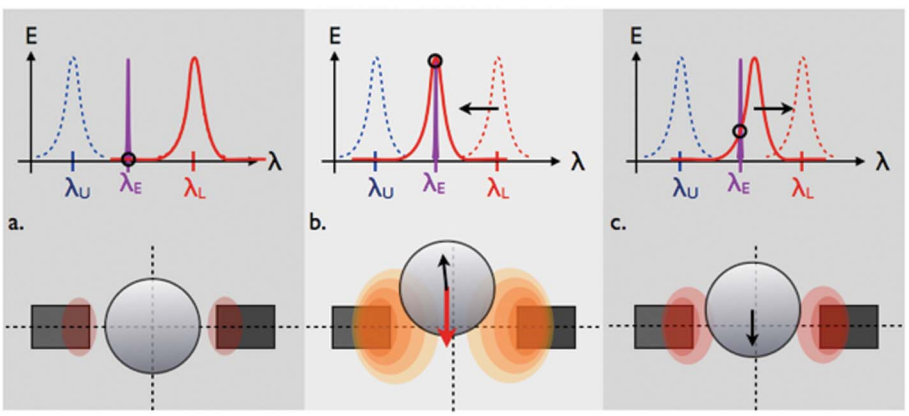

Fig. 5 Illustration of the 1D optical cage. (a) The particle is located at the centre of the cavity. The resonance wavelength shift prevents the detuned excitation from coupling to the optical cavity mode. (b) The particle moves towards the outer region out of Brownian motion. The resonance wavelength shift decreases rapidly leading to a large coupling of energy to the optical mode and the appearance of a strong restoring force. (c) As the particle is driven towards the central region again, light is decoupled from the cavity mode through the same mechanism, leading to the situation described in (a). In all cases the position of the black circle corresponds to the amount of energy coupled to the optical mode at a given time.

 This journal is © The Royal Society of Chemistry 2013

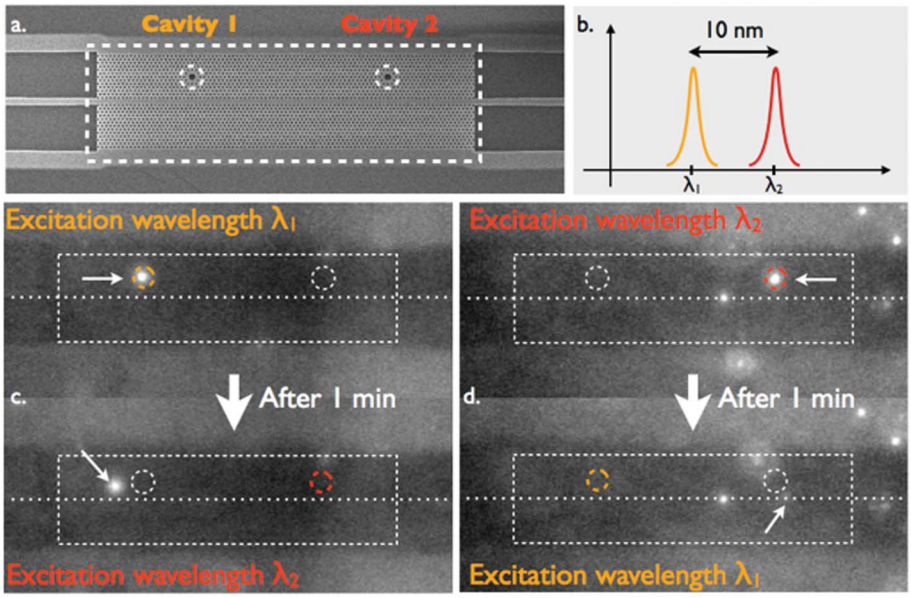

Fig. 6 Addressability of a cavity array. (a) SEM micrograph of a PhC structure comprising of two independent cavities, 720 nm and 700 nm in the diameter for cavity 1 and 2 respectively. (b) Schematic illustration of the spectral separation of the two resonant wavelengths, λ_1 = 1568 nm and λ_2 = 1578 nm. (c) Snapshots demonstrating a particle being trapped in cavity 1 until the excitation wavelength is switched to λ_2, leading to the release of the particle. (d) Similar demonstration as in (c) with cavity 2.

achievable resolution limit for state-of-the-art on-chip spectrometers.[33,34] This property can be used to separate particles of different sizes or to separate particles of identical sizes but of different refractive indices. In the case of the range of values shown in Fig. 7(b), the induced perturbation remains quite small and the shift response is a linear function. As seen from Fig. 7(b), the single particle sensitivity for the detection of a 500 nm particle shows a value of 11 nm/RIU. From this figure, the minimum refractive index change that could be measured with the cavity lies in the order of 0.02 RIU assuming a half-linewidth resolution ($Q_{\text{numerical}}$ = 3300). Fig. 7(c) shows that such a system might also be capable of separating particles that are identical in volume and refractive index but with different form factors.

By performing refractive index measurements, we demonstrate a completely label-free single particle detector platform. Conversely, the HPhC trap approach enables the possibility to capture an unknown particle using a well-chosen detuned wavelength while simultaneously performing optical measurements of the induced perturbation. This can be easily implemented using two lasers, in a "trap and sense" configuration. The size and refractive indices of the particles used in our experiment easily fall within those of a variety of biological entities such as viruses,[2,35,36] cell organelles[37] and small bacteria.[38,39]

A further significant advantage of using HPhC devices to trap particles lies in the inherent scalability of the PhC properties. The sizes and wavelengths can be scaled down to other semiconductor platforms like gallium nitride[40] in the

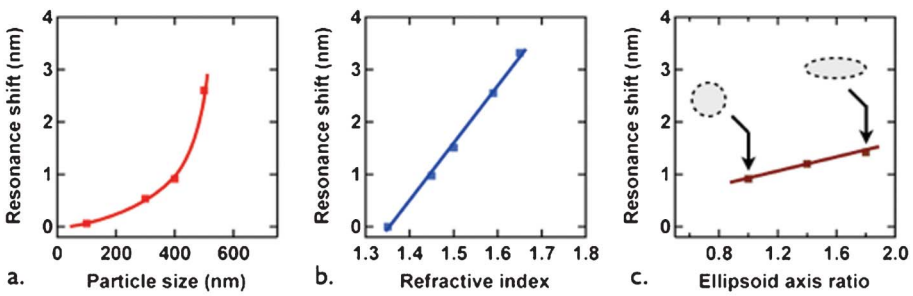

Fig. 7 Computation of the 3D FEM where a particle is placed in the centre of the hollow cavity volume and is displaced along the vertical axis until the particle is far away from the optical near field. The particle-induced perturbation resulting in a resonance shift is computed for (a). Particles of a similar refractive index (1.59) but varying diameters (b). A 500 nm particle with varying refractive index and (c) resonance shift associated with ellipsoidal particles with different aspect ratios but with a constant refractive index (1.59) and volume. The first point on the left corresponds to a 400 nm sphere.

visible wavelength region where the smaller size of the cavity could facilitate the trapping of particles in the order of 50–100 nm.

Conclusions

We have demonstrated a powerful and versatile platform involving an integrated optical resonant trap that can detect and manipulate sub-μm sized particles for extended periods of time with very little optical energy exposure. The simultaneous trapping and induced resonance shifts have potential in new studies such as the refractive index measurement of biological matter such as cell organelles and viruses. The suspended feature of the trap allows the specimen to be unaffected by the surface chemistry. The long trapping times along with very small residual Brownian motion should be of significant interest for studies that use spatially resolved spectroscopy. It could also bring prospects for two- or multi-photon microscopy where the cavity field could be used to generate the fluorescence excitation. The addressability of multiple traps and the compatibility with standard CMOS processes brings immediate access to various exciting on-chip biological analysis applications in the near future.

Acknowledgements

The authors would like to thank Prof. Sebastian Maerkl and his group for their guidance in the conception and fabrication of the microfluidic membrane. The authors acknowledge financial support from the Swiss National Centre of Competence in Research Quantum Photonics and the Swiss National Science Foundation project n° 200021_134541.

References

1 A. Ashkin, J. M. Dziedzic, J. E. Bjorkholm and S. Chu, *Opt. Lett.*, 1986, **11**, 288–290.
2 A. Ashkin and J. Dziedzic, *Science*, 1987, **235**, 1517–1520.
3 E.-L. Florin, A. Pralle, J. K. Heinrich Hörber and E. H. K. Stelzer, *J. Struct. Biol.*, 1997, **119**, 202–211.
4 T. Franosch, M. Grimm, M. Belushkin, F. M. Mor, G. Foffi, L. Forro and S. Jeney, *Nature*, 2011, **478**, 85–88.
5 D. G. Grier, *Nat. Photon.*, 2003, **424**, 810–816.
6 K. Svoboda and S. M. Block, *Annu. Rev. Biophys. Biomol. Struct.*, 1994, **23**, 247–285.
7 A. Ashkin and J. M. Dziedzic, *Proc. Natl. Acad. Sci. U. S. A.*, 1989, **86**, 7914–7918.
8 S. Lin and K. B. Crozier, *Lab Chip*, 2011, **11**, 4047–4051.
9 H. Cai and A. W. Poon, *Lab Chip*, 2012, **12**, 3803–3809.
10 O. G. Helleso, P. Lovhaugen, A. Z. Subramanian, J. S. Wilkinson and B. S. Ahluwalia, *Lab Chip*, 2012, **12**, 3436–3440.
11 A. H. J. Yang, S. D. Moore, B. S. Schmidt, M. Klug, M. Lipson and D. Erickson, *Nature*, 2009, **457**, 71–75.
12 L. Huang, S. J. Maerkl and O. J. Martin, *Opt. Express*, 2009, **17**, 6018–6024.
13 B. S. Schmidt, A. H. Yang, D. Erickson and M. Lipson, *Opt. Express*, 2007, **15**, 14322–14334.
14 S. Mandal, X. Serey and D. Erickson, *Nano Lett.*, 2009, **10**, 99–104.
15 C. Renaut, J. Dellinger, B. Cluzel, T. Honegger, D. Peyrade, E. Picard, F. De Fornel and E. Hadji, *Appl. Phys. Lett.*, 2012, **100**, 101103.
16 K. C. Neuman and A. Nagy, *Nat. Methods*, 2008, **5**, 491–505.
17 M. R. Lee and P. M. Fauchet, *Opt. Lett.*, 2007, **32**, 3284–3286.
18 J. Jágerská, H. Zhang, Z. Diao, N. Le Thomas and R. Houdré, *Opt. Lett.*, 2010, **35**, 2523–2525.
19 A. Di Falco, L. O'Faolain and T. F. Krauss, *Appl. Phys. Lett.*, 2009, **94**, 063503.
20 N. Descharmes, U. Dharanipathy, Z. Diao, M. Tonin and R. Houdré, *Phys. Rev. Lett.*, 2013, **110**, 123601.
21 M. Barth and O. Benson, *Appl. Phys. Lett.*, 2006, **89**, 253114.
22 D. Erickson, D. Sinton and D. Psaltis, *Nat. Photonics*, 2011, **5**, 583–590.
23 Y. C. Seow, S. P. Lim and H. P. Lee, *Lab Chip*, 2012, **12**, 3810–3815.
24 D. Psaltis, S. R. Quake and C. Yang, *Nature*, 2006, **442**, 381–386.
25 C. Monat, P. Domachuk and B. J. Eggleton, *Nat. Photonics*, 2007, **1**, 106–114.
26 Y. Yang, A. Q. Liu, L. K. Chin, X. M. Zhang, D. P. Tsai, C. L. Lin, C. Lu, G. P. Wang and N. I. Zheludev, *Nat. Commun.*, 2012, **3**, 651.
27 D. V. Vezenov, B. T. Mayers, D. B. Wolfe and G. M. Whitesides, *Appl. Phys. Lett.*, 2005, **86**, 041104–041103.
28 A. A. Yanik, M. Huang, O. Kamohara, A. Artar, T. W. Geisbert, J. H. Connor and H. Altug, *Nano Lett.*, 2010, **10**, 4962–4969.
29 M. A. Unger, H.-P. Chou, T. Thorsen, A. Scherer and S. R. Quake, *Science*, 2000, **288**, 113–116.
30 D. W. Prather, A. Sharkawy, S. Shi, J. Murakowski and G. Schneider, *Photonic Crystals, Theory, Applications and Fabrication*, Wiley Publishing, 2009.
31 G.-H. Kim, Y.-H. Lee, A. Shinya and M. Notomi, *Opt. Express*, 2004, **12**, 6624–6631.
32 E. J. G. Peterman, F. Gittes and C. F. Schmidt, *Biophys. J.*, 2003, **84**, 1308–1316.
33 X. Gan, N. Pervez, I. Kymissis, F. Hatami and D. Englund, *Appl. Phys. Lett.*, 2012, **100**, 231104–231104.
34 Z. Xia, A. A. Eftekhar, M. Soltani, B. Momeni, Q. Li, M. Chamanzar, S. Yegnanarayanan and A. Adibi, *Opt. Express*, 2011, **19**, 12356–12364.
35 B. L. Scola, S. Audic, C. Robert, L. Jungang, X. de Lamballerie, M. Drancourt, R. Birtles, J.-M. Claverie and D. Raoult, *Science*, 2003, **299**, 2033.
36 J. A. G. Briggs, T. Wilk, R. Welker, H.-G. Krausslich and S. D. Fuller, *EMBO J.*, 2003, **22**, 1707–1715.
37 S. Bassnett, *Exp. Eye Res.*, 2009, **88**, 133–139.
38 J. Tully, R. Cole, D. Taylor-Robinson and D. Rose, *Lancet*, 1981, **317**, 1288–1291.
39 A. Katz, A. Alimova, X. Min, E. Rudolph, M. K. Shah, H. E. Savage, R. B. Rosen, S. A. McCormick and R. R. Alfano, *IEEE J. Sel. Top. Quantum Electron.*, 2003, **9**, 277–287.
40 N. V. Triviño, G. Rossbach, U. Dharanipathy, J. Levrat, A. Castiglia, J. F. Carlin, K. A. Atlasov, R. Butté, R. Houdré and N. Grandjean, *Appl. Phys. Lett.*, 2012, **100**, 071103–071103.

 This journal is © The Royal Society of Chemistry 2013